

*Supporting Information for:*

**From Ionic Liquid-Modified Cellulose Nanowhiskers to Highly Active Metal-Free  
Nanostructured Carbon Catalysts for Hydrazine Oxidation Reaction**

*Elizângela H. Fragal,<sup>a,b</sup> Vanessa H. Fragal,<sup>a,b</sup> Xiaoxi Huang,<sup>b</sup> Alessandro C. Martins,<sup>a,b</sup> Thelma Sley P. Cellet,<sup>a</sup> Guilherme M. Pereira,<sup>a</sup> Eliška Mikmeková,<sup>c</sup> Adley F. Rubira,<sup>a</sup> Rafael Silva<sup>a\*</sup> and Tewodros Asefa<sup>b,d\*</sup>*

a. Departamento de Química, Universidade Estadual de Maringá, Avenida Colombo 5790, CEP: 87020-900, Maringá, Paraná, Brazil.

b. Department of Chemistry and Chemical Biology, Rutgers, The State University of New Jersey, Piscataway, 610 Taylor Road, New Jersey 08854, United States.

<sup>c</sup> Institute of Scientific Instruments of the ASCR, Královopolská 147, Brno 612 64, Czech Republic.

d. Department of Chemical and Biochemical Engineering, Rutgers, The State University of New Jersey, 98 Brett Road, Piscataway, New Jersey 08854, United States.

Corresponding Authors' E-mails: (TA) [tasefa@rci.rutgers.edu](mailto:tasefa@rci.rutgers.edu); (RS) [rsilva2@uem.br](mailto:rsilva2@uem.br)

**Keywords:** cellulose nanowhiskers, ionic liquid, hydrazine oxidation, electrocatalysis, carbon nanomaterial

## **Electrocatalysis Experiments**

**Preparation of working electrodes.** The electrocatalytic properties of the materials were evaluated with a Versastat3 potentiostat (Princeton Applied Research, PAR) instrument using a three-electrode cell. The cell consisted of a 3 mm diameter glassy carbon (GC) disk coated with the prepared carbon materials as the working electrode, a graphitic carbon (diameter: 0.5 mm) as the counter electrode, and a saturated calomel electrode (SCE) as the reference electrode.

To prepare the working electrode, 4 mg of each material was dispersed in a solution containing 205  $\mu\text{L}$  of 2-propanol, 610  $\mu\text{L}$  of water and 86  $\mu\text{L}$  of 5% Nafion with sonication. Then, 1.6  $\mu\text{L}$  of the suspension was pipetted onto the surface of a glassy carbon disc electrode (GC) disk. After letting it to dry under ambient conditions, the electrode became ready to use.

**Cyclic voltammetry.** The hydrazine oxidation reaction (HOR) over the carbon materials was analyzed by cyclic voltammetry (CV) in a 0.1 M phosphate buffered saline (PBS) at pH = 7.4. The potential was scanned from -0.6 to 0.6 vs. SCE at a scan rate of 10 mV/s for different concentrations of hydrazine ranging between 10 mM to 50 mM.

**Chronoamperometry.** The chronoamperometry analysis of HOR over the samples was measured at a potential of -0.10 V vs. SCE in the presence of 50 mM hydrazine.

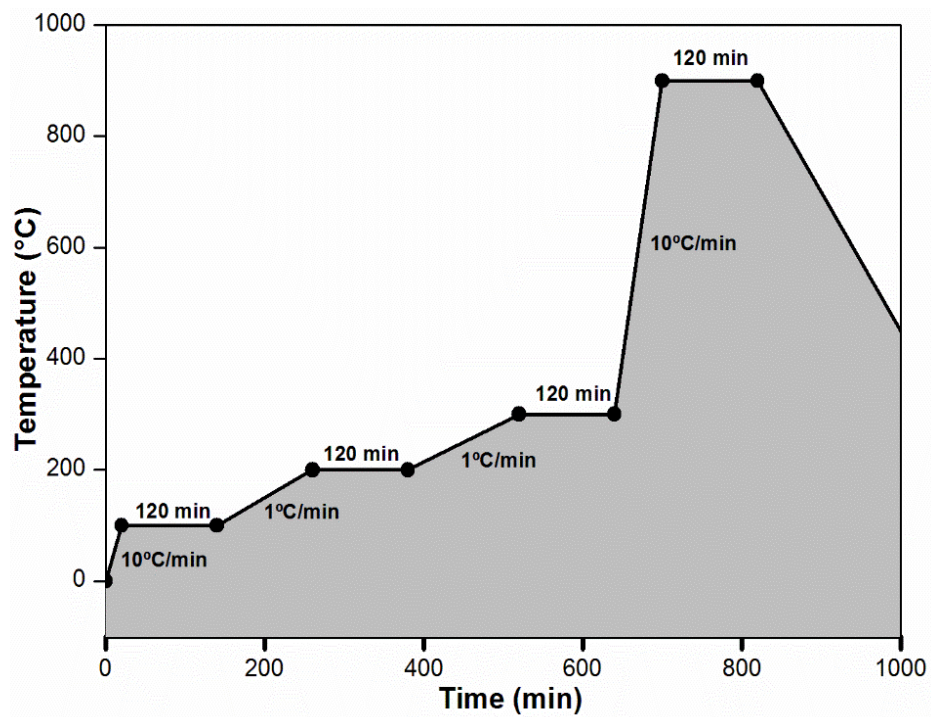


**Figure S1.** The thermal treatment steps applied on the various CNWs-based precursors to produce the different carbon materials synthesized and studied in the work.

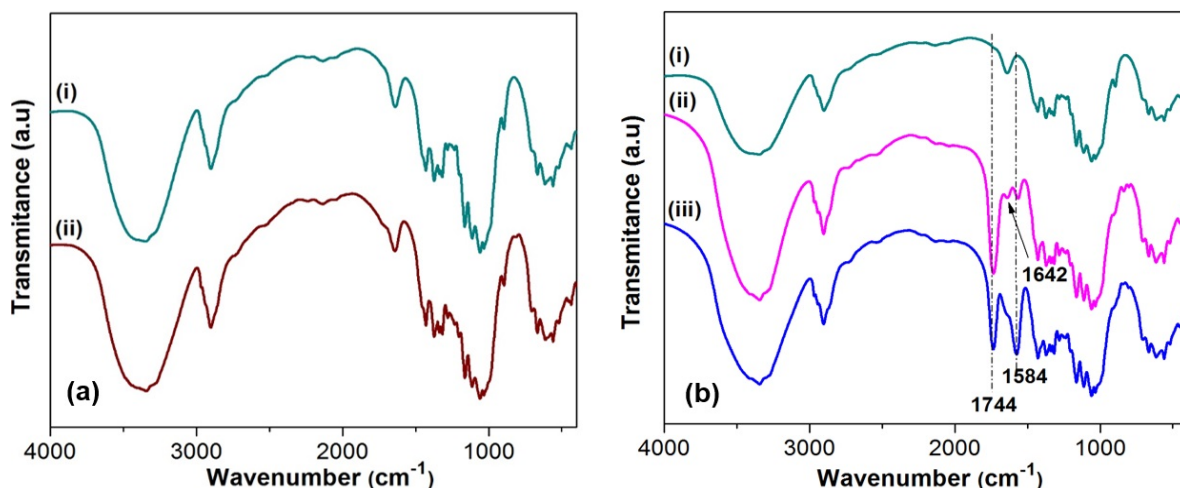


**Figure S2.** (a) FTIR spectra of: (i) cellulose after hydrolysis with HCl, producing a product named as CNWh, (ii) cellulose after hydrolysis with H<sub>2</sub>SO<sub>4</sub> (or CNWs-SO<sub>3</sub><sup>-</sup>). (b) FTIR spectra of CNWh (i) before it is let to react with succinic anhydride, (ii) after it is let to react with succinic anhydride (producing a material denoted as CNWsa), and (iii) after the CNWsa is subjected to deprotonation, producing carboxylate-functionalized CNWs (denoted here as CNWs-CO<sub>2</sub><sup>-</sup>).

For cellulose hydrolyzed with HCl and H<sub>2</sub>SO<sub>4</sub>, there are no significant differences between the FTIR spectra of the hydrolyzed products. As expected, IR bands corresponding to SO<sub>3</sub><sup>-</sup> groups are not observable in the spectra.<sup>1</sup> Their presence was supported by elemental analysis and TGA below. In Figure S2(b), the spectra of CNWs modified with carboxylate groups are shown. A strong band at around 1744 cm<sup>-1</sup> due to the absorption by carbonyl groups of esters and carboxylic acids is shown in (ii) of Figure S2(b). The band at 1638 cm<sup>-1</sup> is attributed to the bending mode of physisorbed water in the materials. Finally, a band at 1584 cm<sup>-1</sup> is attributed to the antisymmetric stretching of carboxylic groups.<sup>2,3</sup>

The XRD results performed in the celluloses and the hydrolyzed cellulose generally reveal that the original CNWs are highly crystalline, but lose some of their crystallinity after treatment with IL. For example, the original CNWs prepared using sulfuric acid (CNWs-SO<sub>3</sub><sup>-</sup>) are crystalline with 86.1 % crystallinity, but they show lower crystallinity with a value of 74.1 % after treatment with [C<sub>4</sub>mim][CH<sub>3</sub>SO<sub>3</sub>]. Similarly, CNWs-CO<sub>2</sub><sup>-</sup> are highly crystalline with a value of 83.3 % crystallinity but after treatment with the IL, their crystallinity index decreases to a value of 65.9 %. The decrease in crystallinity by *ca.* 12 % in CNWs-SO<sub>3</sub><sup>-</sup> and by *ca.* 17 % in CNWs-CO<sub>2</sub><sup>-</sup> suggests the penetration of IL into the crystalline structure of cellulose in the CNWs.”

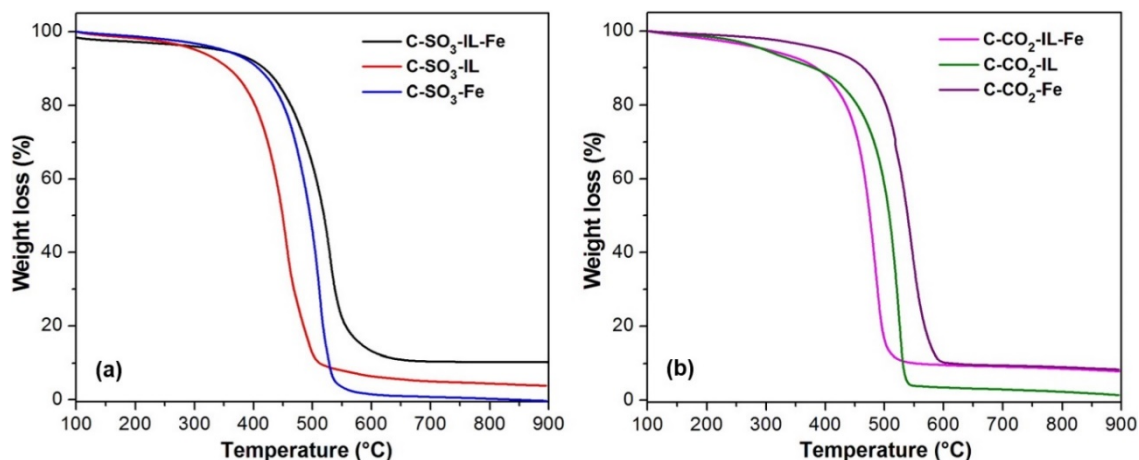


**Figure S3.** (a) Thermogravimetric analysis (TGA) curves of C-SO<sub>3</sub>-IL-Fe, C-SO<sub>3</sub>-IL, and C-SO<sub>3</sub>-Fe. (b) TGA curves of C-CO<sub>2</sub>-IL-Fe, C-CO<sub>2</sub>-IL, and C-CO<sub>2</sub>-Fe. IL represents [C4mim].

When comparing the TGA results of the samples derived from CNWs-SO<sub>3</sub><sup>-</sup> amongst one another, it can be seen that C-SO<sub>3</sub>-[C4mim]-Fe and C-SO<sub>3</sub>-Fe are stable up to about 380 °C and C-SO<sub>3</sub>-[C4mim] is stable only up to about 350 °C. This indicates the relatively higher thermal stability of the materials containing, or made with, Fe species. The highest value of residual weight (%) is found for C-SO<sub>3</sub>-[C4mim]-Fe material, indicating that this sample contains the highest amount of Fe-based species compared with all the others.

Compared with the CNWs-SO<sub>3</sub><sup>-</sup>-derived materials, all the material made from CNW-CO<sub>2</sub><sup>-</sup> are more thermally stable, showing onset degradation temperatures higher than 400 °C. This may be due to the higher crystallinity of the precursors of the former compared with those of the latter. Nevertheless, the results overall suggest also that the thermal stability of the carbon materials derived from CNWs can be indirectly dictated by the hydrolysis process employed and the surface functional groups present on their cellulose precursors.

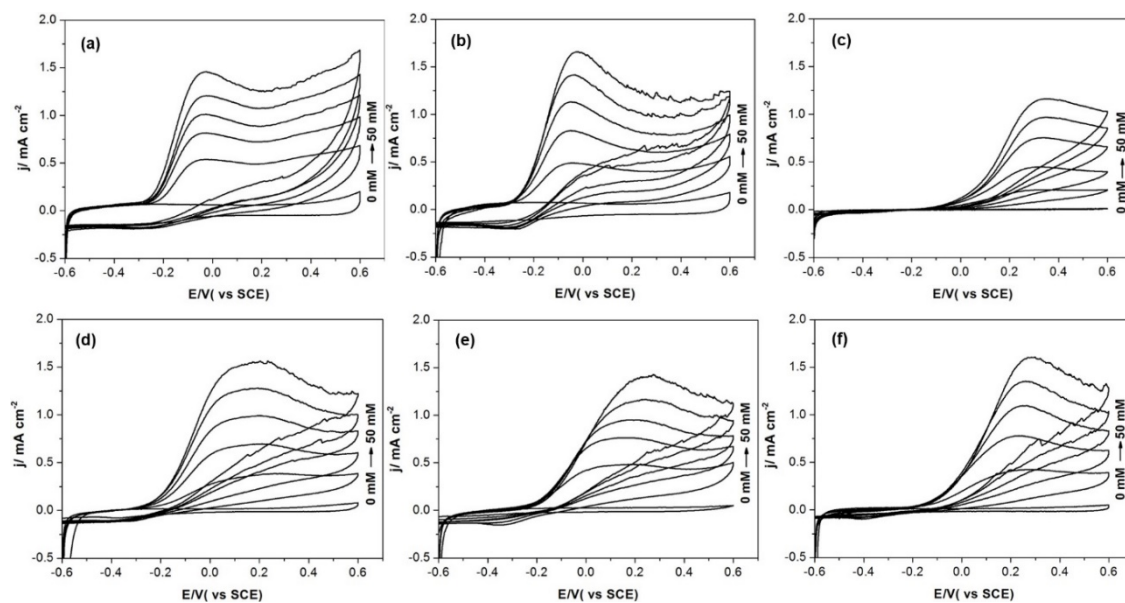


**Figure S4.** Cyclic voltammograms (CVs) of HOR obtained at a scan rate of  $10 \text{ mV}^{-1}$  for different concentrations of hydrazine (10 mM to 50 mM) in 0.1 M PBS using over the different carbon materials synthesized and studied: (a) C-SO<sub>3</sub>-[C4mim]-Fe, (b) C-SO<sub>3</sub>-[C4mim], (c) C-SO<sub>3</sub>-Fe, (d) C-CO<sub>2</sub>-[C4mim]-Fe, (e) C-CO<sub>2</sub>-[C4mim], and (f) C-CO<sub>2</sub>-Fe.

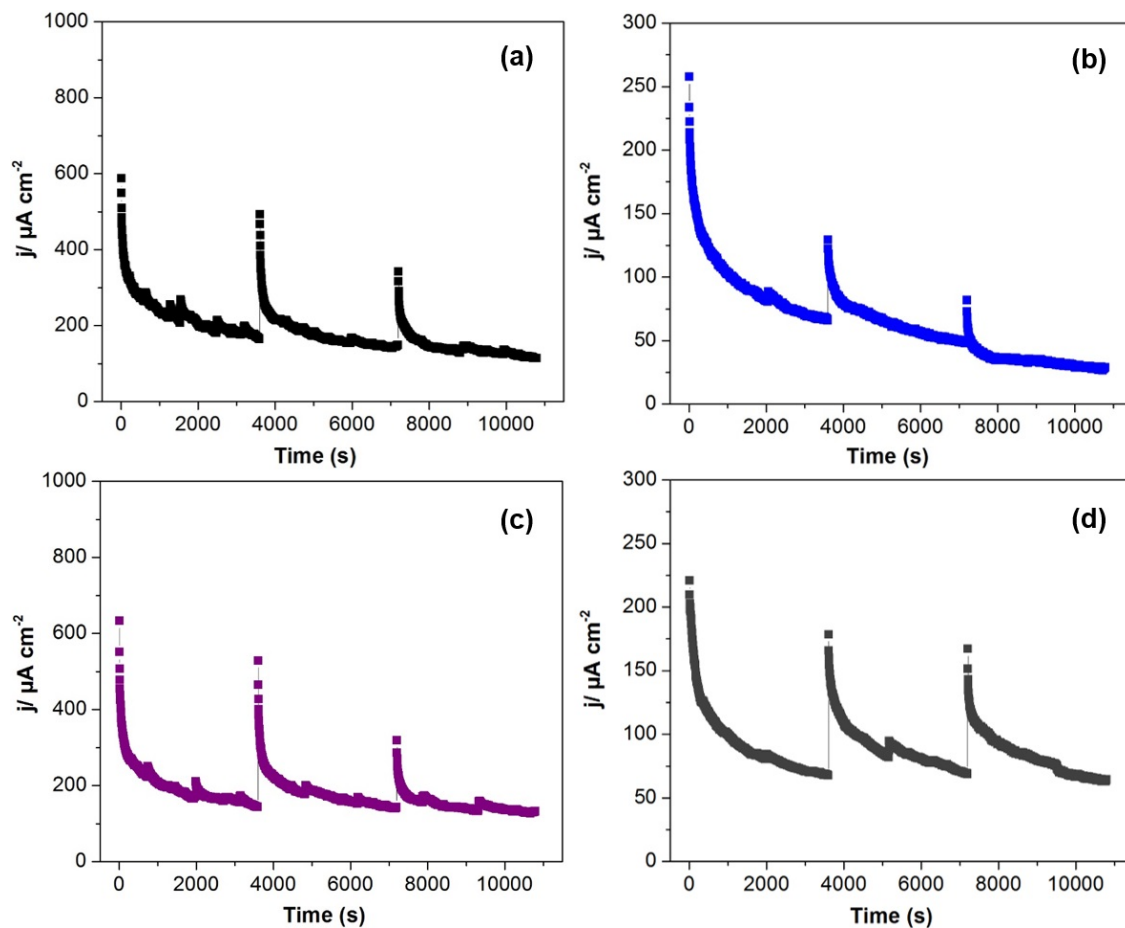


**Figure S5.** Chronoamperometry results for HOR over (a)  $\text{C-SO}_3\text{-[C4mim]-Fe}$ , (b)  $\text{C-SO}_3\text{-Fe}$ , (c)  $\text{C-CO}_2\text{-[C4mim]-Fe}$ , and (d)  $\text{C-CO}_2\text{-Fe}$  over long reaction times.

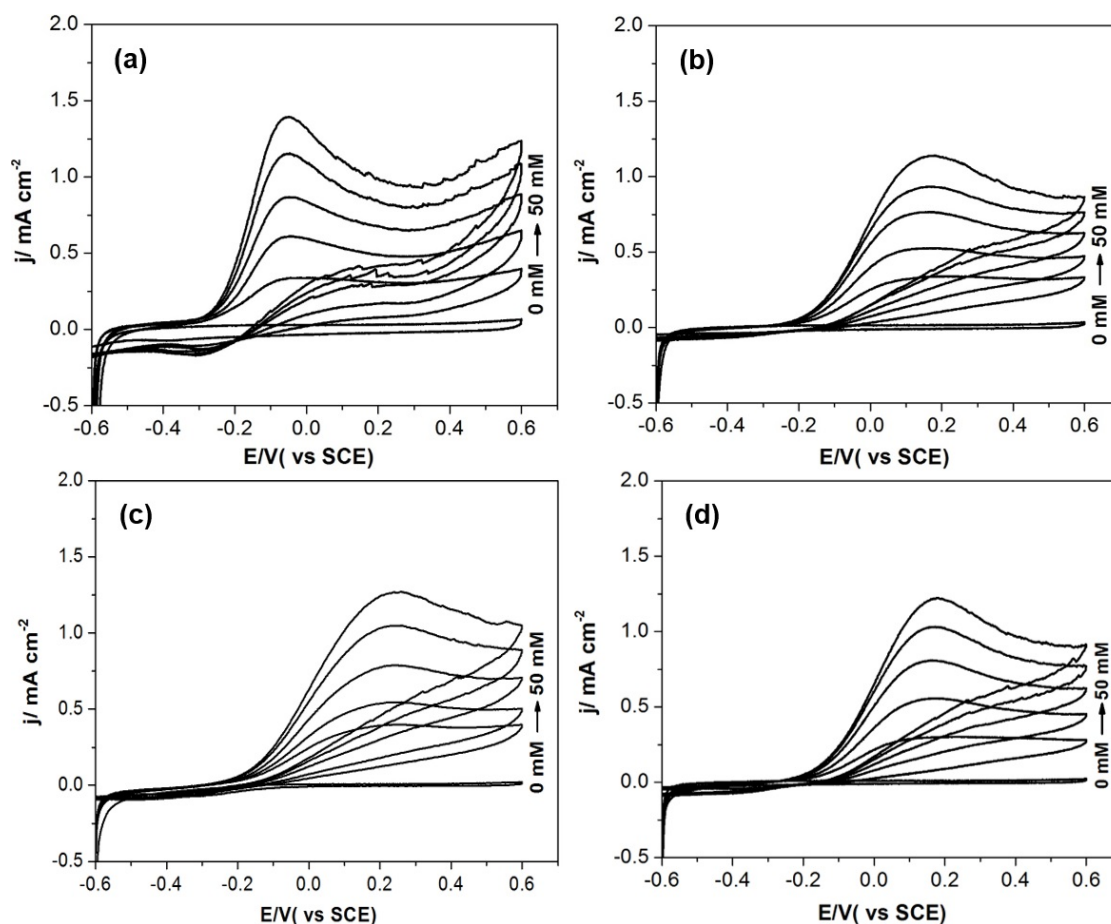


**Figure S6.** Cyclic voltammograms of HOR at  $10 \text{ mV}^{-1}$  in  $0.1 \text{ M}$  PBS using different concentrations of hydrazine ( $10 \text{ mM}$ - $50 \text{ mM}$ ) over the Fe-containing carbon materials after being treated with  $1 \text{ M}$   $\text{HNO}_3$  for 24 hours. The samples include: (a)  $\text{C-SO}_3\text{-[C4mim]-Fe}^{\text{R}}$  (b)  $\text{C-SO}_3\text{-Fe}^{\text{R}}$  (c)  $\text{C-CO}_2\text{-[C4mim]-Fe}^{\text{R}}$  (d)  $\text{C-CO}_2\text{-Fe}^{\text{R}}$ , where R stands for “removal” of Fe.

After stirring the carbon materials containing Fe (*i.e.*,  $\text{C-SO}_3\text{-[C4mim]-Fe}$ ,  $\text{C-SO}_3\text{-Fe}^{\text{R}}$ ,  $\text{C-CO}_2\text{-[C4mim]-Fe}$ , and  $\text{C-CO}_2\text{-Fe}$ ) with  $1 \text{ M}$   $\text{HNO}_3$  for 24 h, and removing their Fe species off of them, the corresponding materials labeled as  $\text{C-SO}_3\text{-[C4mim]-Fe}^{\text{R}}$ ,  $\text{C-SO}_3\text{-Fe}^{\text{R}}$ ,  $\text{C-CO}_2\text{-[C4mim]-Fe}^{\text{R}}$  and  $\text{C-CO}_2\text{-Fe}^{\text{R}}$  materials are obtained. The electrocatalytic activities of the latter are found to be slightly lower than those of their corresponding original ones.



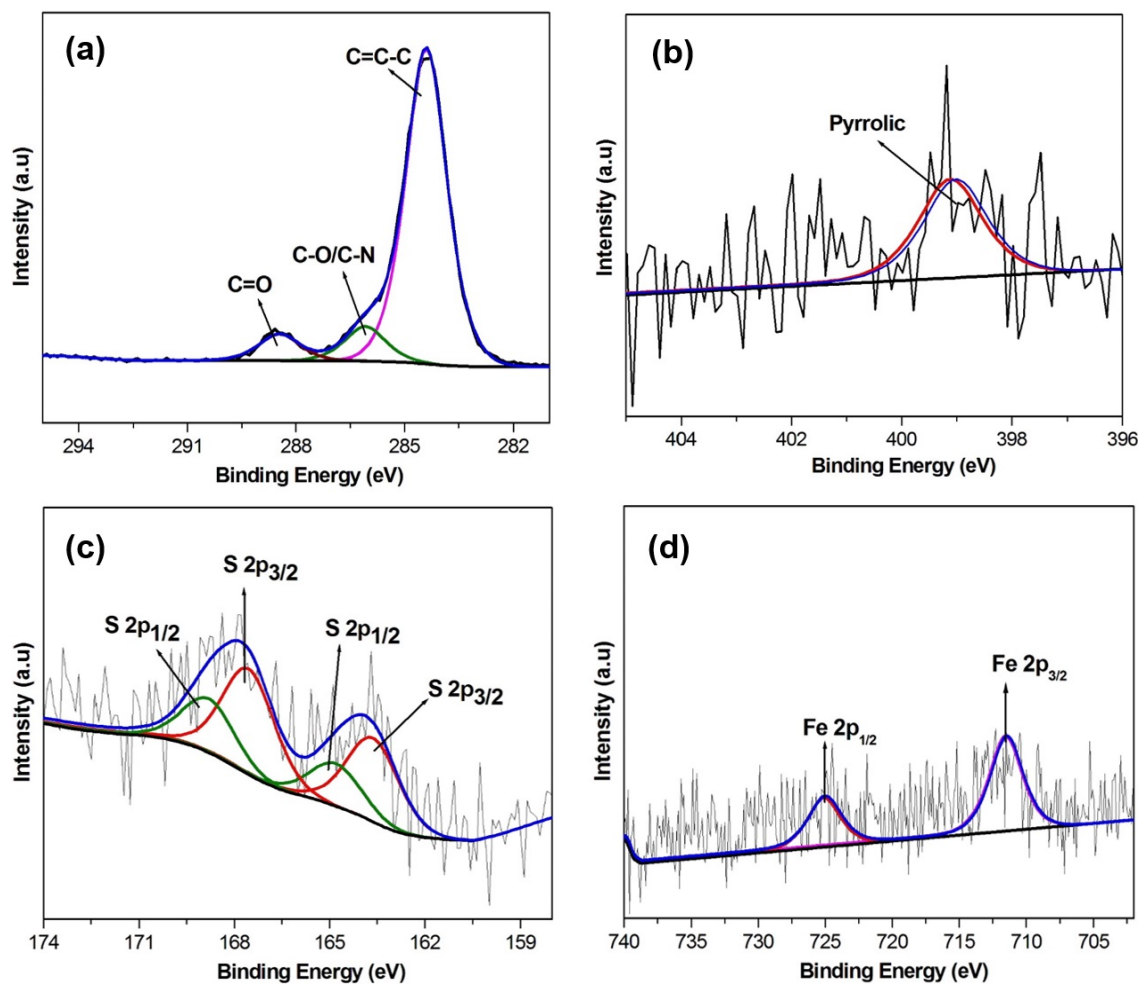


**Figure S7.** High-resolution XPS spectra of the (a) C1s, (b) N1s, (c) S2p, and (d) Fe2p peaks of C-SO<sub>3</sub>-[C4mim]-Fe material.

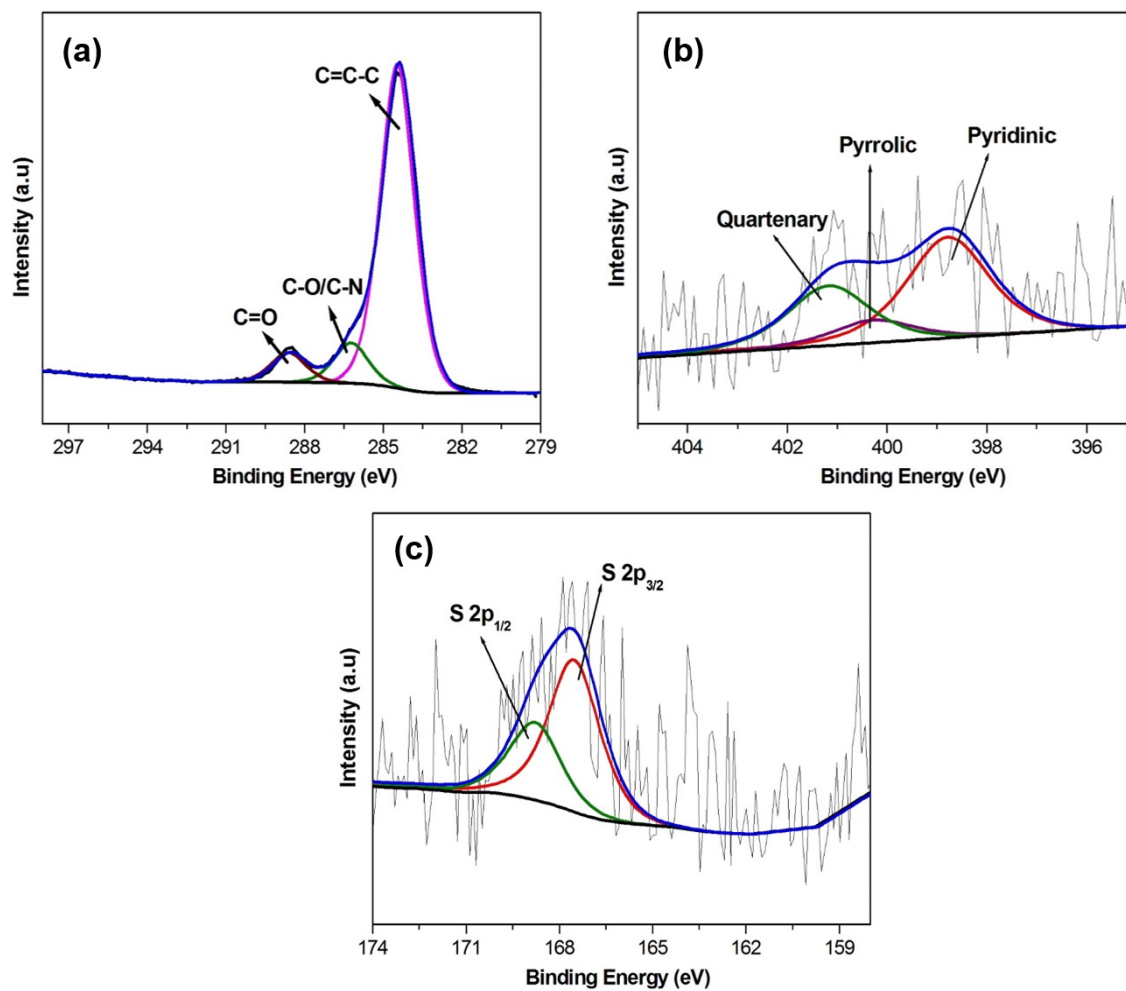


**Figure S8.** High-resolution XPS spectra of the (a) C1s, (b) N1s, and (c) S2p peaks of C-SO<sub>3</sub>-[C4mim] material.

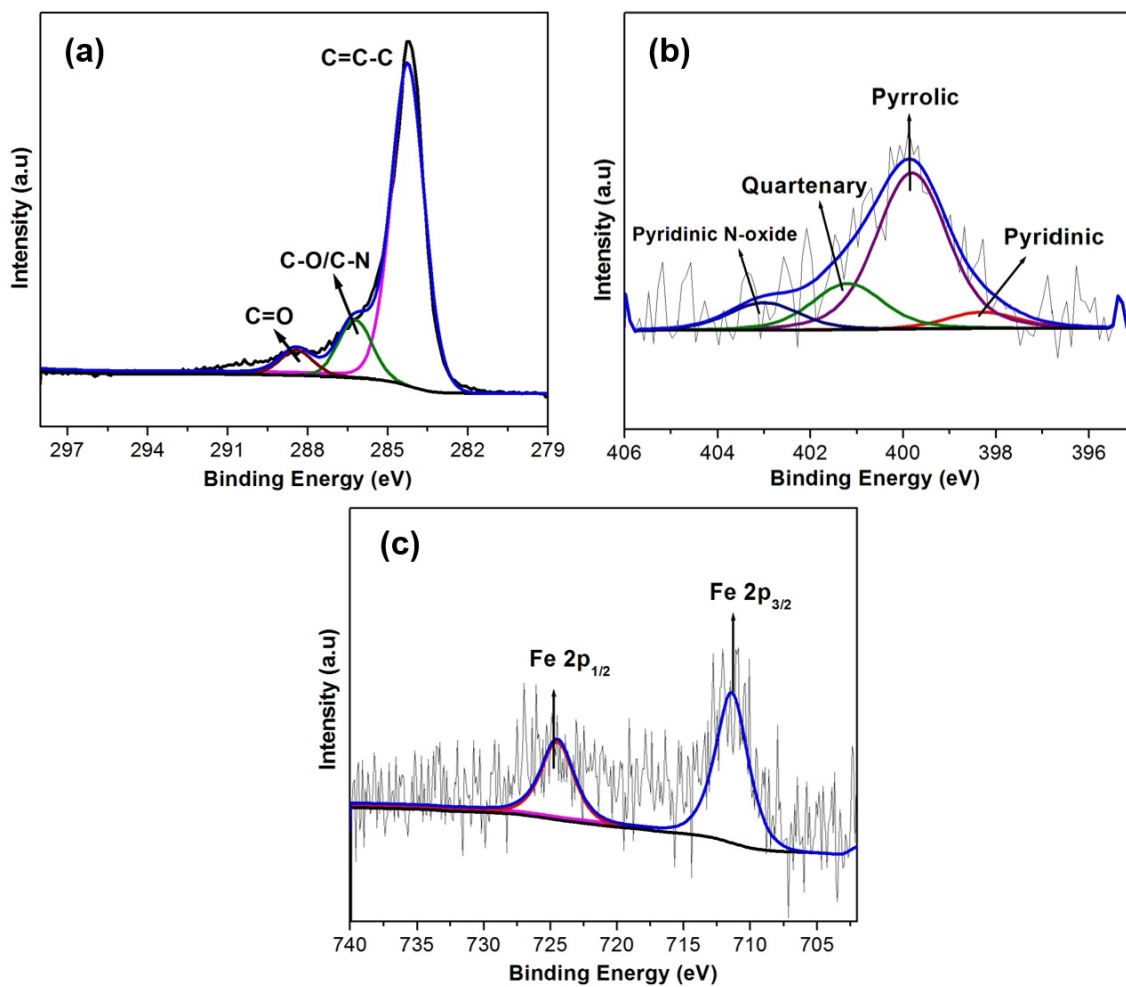


**Figure S9.** High-resolution XPS spectra of the (a) C 1s, (b) N 1s, (c) S 2p, and (d) Fe2p peaks of C-SO<sub>3</sub>-Fe material.

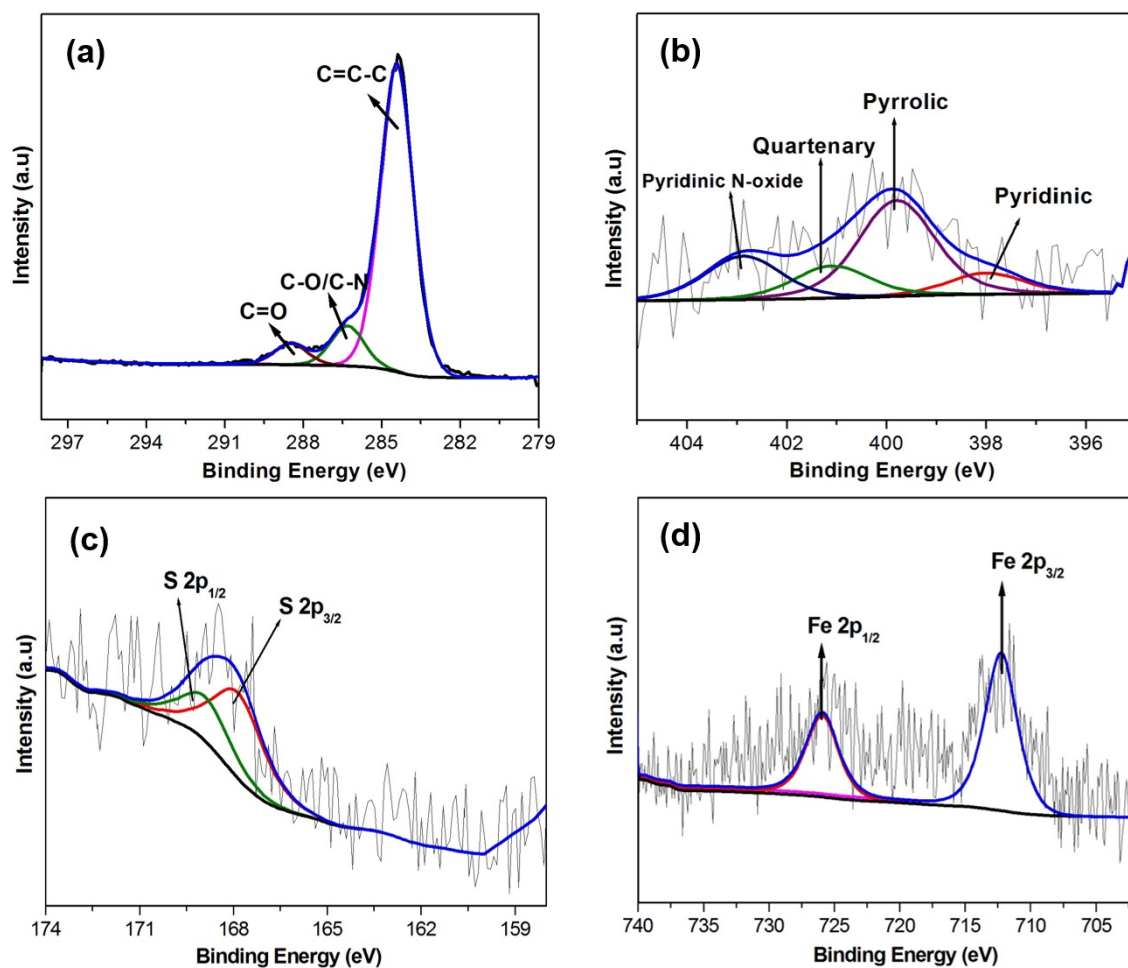


**Figure S10.** High-resolution XPS spectra of the (a) C1s, (b) N1s, (c) S2p, and (d) Fe2p peaks of C-CO<sub>2</sub>-[C4mim]-Fe material.

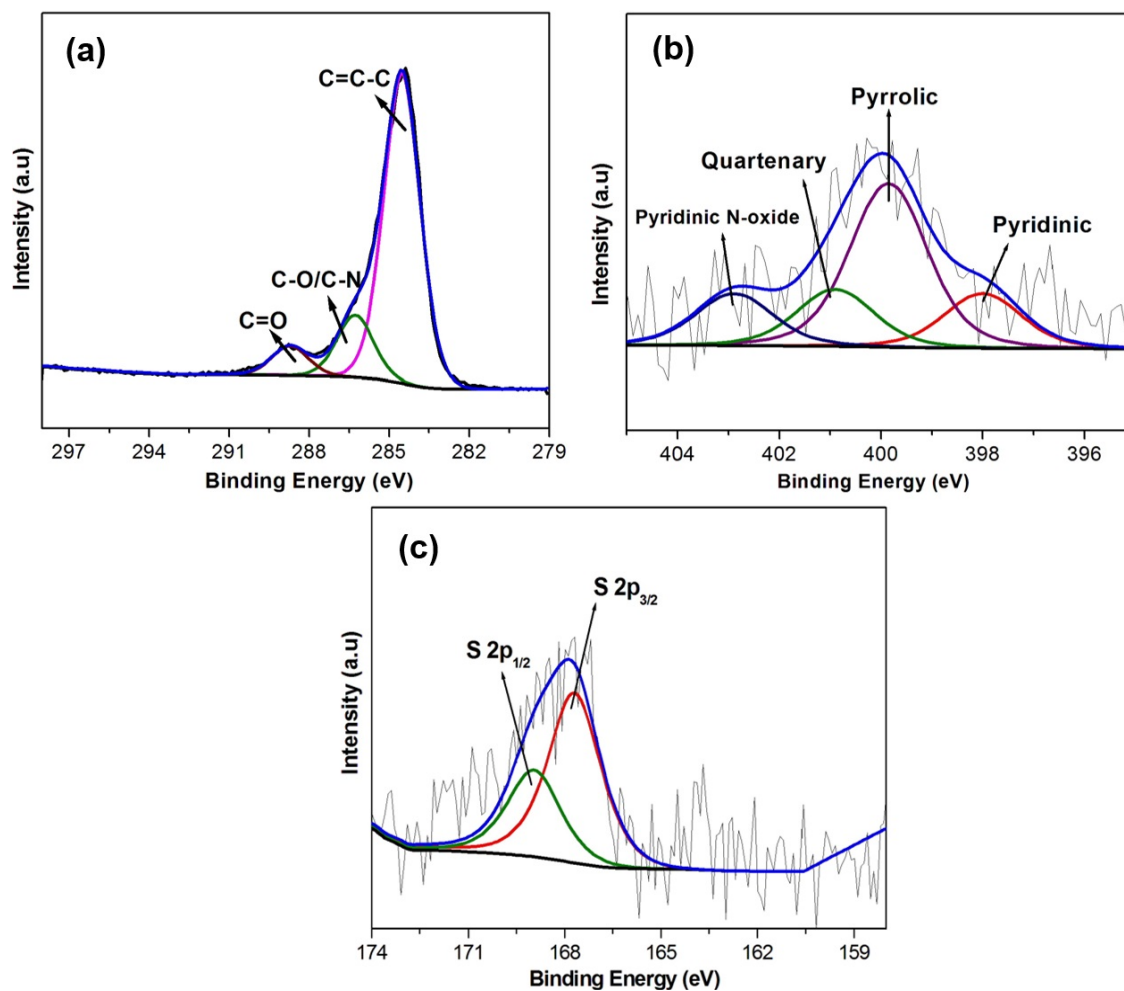


**Figure S11.** High-resolution XPS spectra of the (a) C1s, (b) N1s, and (c) S2p peaks of C-CO<sub>2</sub>-[C4mim] material.

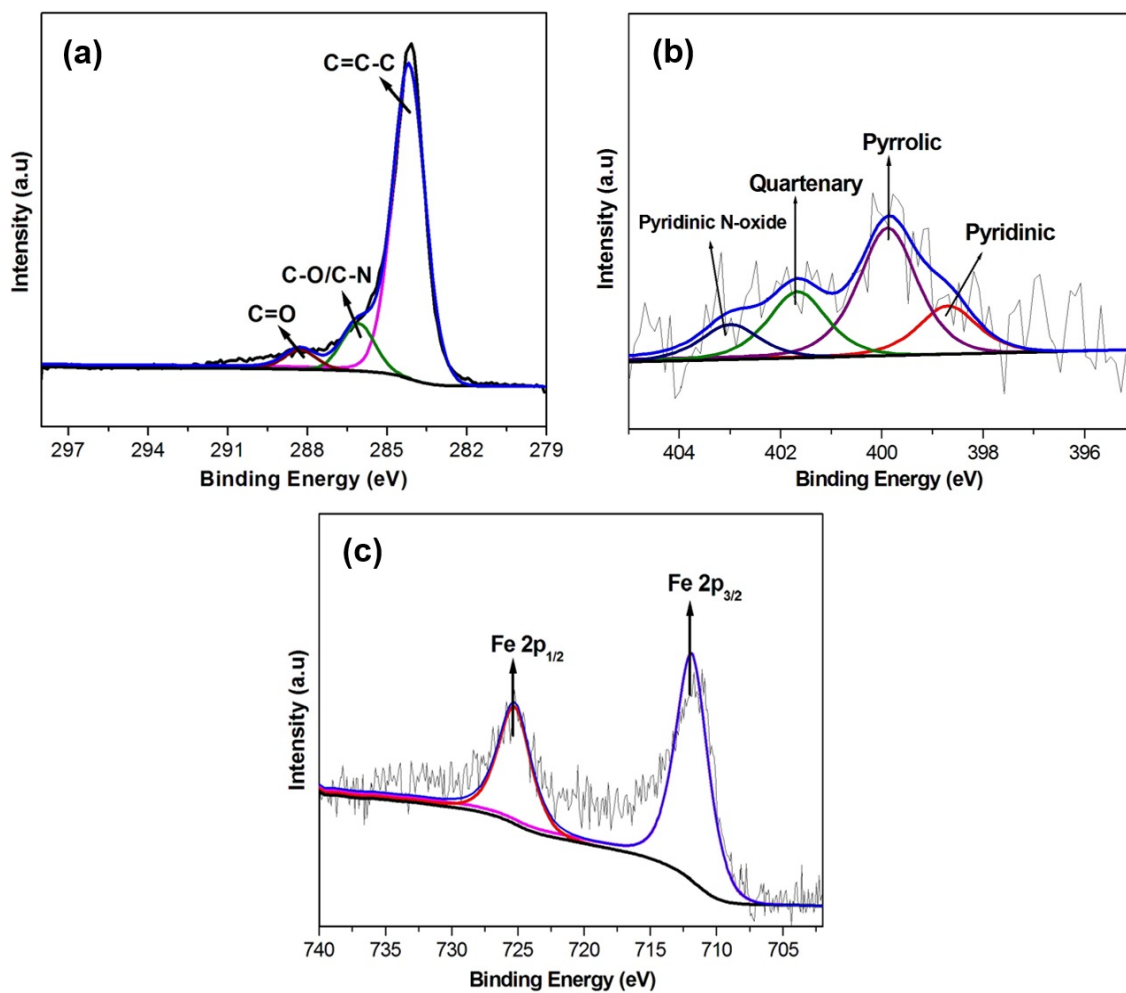


**Figure S12.** High-resolution XPS spectra of the (a) C1s, (b) N1s, (c) S2p, and (d) Fe2p peaks of C-CO<sub>2</sub>-Fe material.

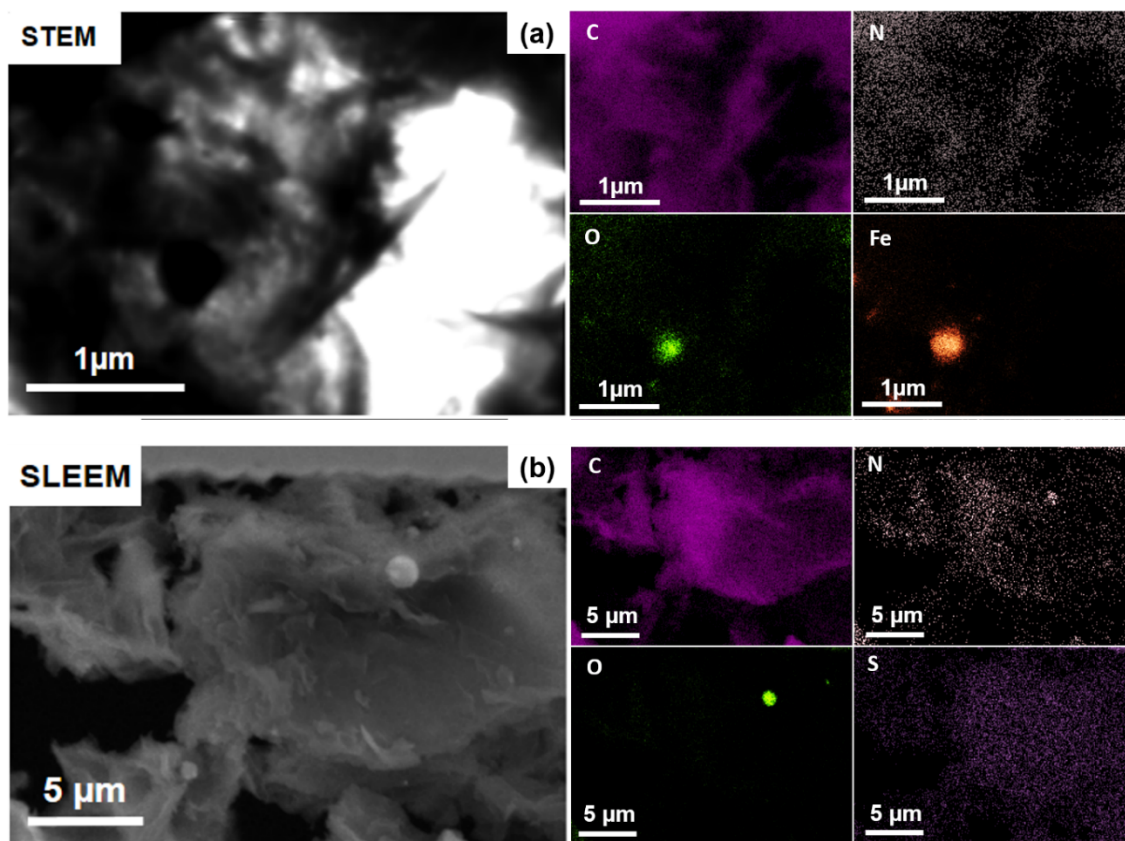


**Figure S13.** (a) (Left Panel) STEM image and (Right Panel) elemental mapping images of C, N, O and Fe atoms of C-SO<sub>3</sub>-Fe. (b) (Left Panel) SLEEM image and (Right Panel) elemental mapping images of C, N, O and S atoms of C-CO<sub>2</sub>-[C4mim][CH<sub>3</sub>SO<sub>3</sub>].

**Table S1.** Comparison of results of the catalytic activities toward HOR of different materials recently reported in the literature with the current work.

Electrocatalyst	Medium	Scan rate (mV s <sup>-1</sup> )	[N <sub>2</sub> H <sub>4</sub> ] mM	Onset/Peak Potential (V vs.SCE)	Reference
<b>C-SO<sub>3</sub>- [C<sub>4</sub>mim]</b>	<b>PBS</b>	<b>10</b>	<b>50</b>	<b>-0.29 / -0.03</b>	<b>This work</b>
<b>PPY-NOMPC- 900</b>	PBS	10	50	- 0.36 / -0.06	4
<b>Metal free- carbon nanoneedles</b>	PBS	20	10	0.15 / 0.1	5
<b>Nitrogen doped holey graphene</b>	PBS	20	10	- 0.15 / 0.35	6
<b>PCDF-900</b>	PBS	10	50	-0.30 / 0.1	7
<b>Au/TiO<sub>2</sub>- NTs/Ti</b>	PBS	100	0.85	- 0.10 / 0.24	8
<b>Ag/CFC</b>	KOH	10	20	-0.5 / -0.2 <sup>a</sup>	9
<b>ASP-Ni</b>	NaOH	-	100	0.5 / 0.24 <sup>b</sup>	10
<b>Flower-shaped CuO</b>	KOH	50	10	-0.14 / 0.22 <sup>a</sup>	11
<b>Pd-NWNWs</b>	HClO <sub>4</sub>	50	10	0.25 / 0.46 <sup>b</sup>	12
<b>AuPd DANCs</b>	HClO <sub>4</sub>	50	10	-0.11 / 0.1	13
<b>Au(Ni)/TiO<sub>2</sub>- NTs</b>	NaOH	10	50	-0.42 / 0.2 <sup>a</sup>	14

<sup>a</sup> vs. Ag/AgCl, KCl-sat.; <sup>b</sup> E/V vs. RHE



**Table S2.** XPS data compiled for all carbon materials prepared from CNWs-SO<sub>3</sub><sup>-</sup> or CNWs-CO<sub>2</sub><sup>-</sup> with and without IL and Fe(III) ions. Please note that the samples were then coated with silica shells, subjected to carbonization, and treated with NaOH solution to remove their silica shells.

Materials	Elements										
	C 1s			O 1s	N 1s				Fe 2p <sub>3/2</sub>	S 2p <sub>3</sub>	
	C=C-C	C-O /C-N	C=O		C-N	C=NH	N <sup>+</sup> -C4	N <sup>+</sup> -O <sup>-</sup>			
C-SO <sub>3</sub> -IL-Fe	284.4	286.1	288.4	531.7/ 533.1	/	399.1	/	/	711.4	163.6/ 167.5	Binding Energy (eV)
	69.2	7.6	5.8	16.7	/	0.18	/	/	0.12	0.2	Atomic percentage (%)
C-SO <sub>3</sub> -IL	284.3	286.1	288.5	531.8 533.1	398.6	400.1	401.1	/	/	167.4	Binding Energy (eV)
	70.3	8.7	6.4	13.7	0.35	0.08	0.2	/	/	0.12	Atomic percentage (%)
C-SO <sub>3</sub> -Fe	284.2	286.2	288.4	531.9/ 544.9	398.5	399.8	401.1	/	711.3	/	Binding Energy (eV)
	71.2	12.1	5.2	10.1	0.23	0.59	0.34	/	0.22	/	Atomic percentage (%)
C-CO <sub>2</sub> -IL-Fe	284.4	286.3	288.4	531.8	398.6	/	400.3	/	712.2	167.8	Binding Energy (eV)
	62.8	8.3	4.4	22.9	0.25	/	0.61	/	0.33	0.19	Atomic percentage (%)
C-CO <sub>2</sub> -IL	284.5	286.2	288.7	532.2	398.6	399.9	401.3	/	/	167.7	Binding Energy (eV)
	63.7	12.8	6.1	15.9	0.22	0.76	0.27	/	/	0.28	Atomic percentage (%)
C-CO <sub>2</sub> -Fe	284.1	286.1	288.2	531.1/ 532.6	398.7	399.8	401.6	403.1	711.8	167.3	Binding Energy (eV)
	67.7	9.9	3.9	16.1	0.17	0.45	0.23	0.12	1.05	/	Atomic percentage (%)

\*IL represents [C4mim][CH<sub>3</sub>SO<sub>3</sub>].

## References

1. J. Gu, J. M. Catchmark, E. Q. Kaiser and D. D. Archibald, *Carbohydr. Polym.*, 2013, **92**, 1809-1816.
2. B. Belhafaoui, A. Aziz, H. Elandaloussi el, M. S. Ouali and L. C. De Menorval, *J. Hazard. Mater.*, 2009, **169**, 831-837.
3. J. C. P. Melo, E. C. Silva Filho, S. A. A. Santana and C. Airoidi, *Thermochim. Acta*, 2011, **524**, 29-34.
4. Y. Meng, X. Zou, X. Huang, A. Goswami, Z. Liu and T. Asefa, *Adv. Mater.*, 2014, **26**, 6510-6516.
5. R. Silva, J. Al-Sharab and T. Asefa, *Angew. Chem. Int. Ed.*, 2012, **51**, 7171-7175.
6. D. Yu, L. Wei, W. Jiang, H. Wang, B. Sun, Q. Zhang, K. Goh, R. Si and Y. Chen, *Nanoscale*, 2013, **5**, 3457-3464.
7. A. C. Martins, X. Huang, A. Goswami, K. Koh, Y. Meng, V. C. Almeida and T. Asefa, *Carbon*, 2016, **102**, 97-105.
8. M. Hosseini, M. M. Momeni and M. Faraji, *J. Mol. Catal. A: Chem.*, 2011, **335**, 199-204.
9. R. Liu, K. Ye, Y. Gao, W. Zhang, G. Wang and D. Cao, *Electrochim. Acta*, 2015, **186**, 239-244.
10. T.-Y. Jeon, M. Watanabe and K. Miyatake, *ACS Appl. Mater. Interfaces*, 2014, **6**, 18445-18449.
11. Y. Ma, H. Wang, J. Key, S. Ji, W. Lv and R. Wang, *J. Power Sources*, 2015, **300**, 344-350.
12. F. Li, Y. Ji, S. Wang, S. Li and Y. Chen, *Electrochim. Acta*, 2015, **176**, 125-129.
13. L.-X. Chen, L.-Y. Jiang, A.-J. Wang, Q.-Y. Chen and J.-J. Feng, *Electrochim. Acta*, 2016, **190**, 872-878.
14. L. Tamašauskaitė-Tamašiūnaitė, J. Rakauskas, A. Balčiūnaitė, A. Zabielaite, J. Vaičiūnienė, A. Selskis, R. Juškėnas, V. Pakštas and E. Norkus, *J. Power Sources*, 2014, **272**, 362-370.